Journal of Alloys and Compounds 785 (2019) 391–397

Contents lists available at ScienceDirect

Journal of Alloys and Compounds

journal homepage: http://www.elsevier.com/locate/jalcom

Influence of controlled Pd nanoparticles decorated TiO_2 nanowire arrays for efficient photoelectrochemical water splitting

Jingjing He, Meng Wang, Xiaofeng Wu, Yu Sun, Keke Huang, Huanwen Chen, Lu Gao*, Shouhua Feng

State Key Laboratory of Inorganic Synthesis and Preparative Chemistry, College of Chemistry, Jilin University, Changchun, 130012, PR China

ARTICLE INFO

Article history:
Received 11 December 2018
Received in revised form
9 January 2019
Accepted 16 January 2019
Available online 17 January 2019

Keywords:
Pd nanoparticles
Electrospray technique
Photoelectrochemical water splitting
Schottky contact

ABSTRACT

This work depicts the synthesis of controllable Pd nanoparticles decorated TiO_2 nanowire arrays by electrospray technique. By varying the substrate temperature and volume of precursor solution, Pd/TiO_2 hybrid structure with different sizes and deposition yield was precisely controlled. The highest photocurrent density of the Pd/TiO_2 photoanode was 1.4 mA cm^{-2} at 1.23 V vs. RHE, which was approximately 5 times higher than the pristine TiO_2. The onset potential with a significant cathodic shift of 80 mV compared to the pristine TiO_2 was also observed. To the best of our knowledge, the obtained photocurrent showed the optimal photocurrent density and high stability compared with previous reports. It is also found that the photoelectrochemical performance is closely related to the size and deposition quantity of Pd nanoparticles. According to the results, the enhanced PEC performance can be attributed to the Schottky junction, charge transfer and the enhancement about the separation efficiency of the photogenerated electrons and holes betweenTiO_2 and Pd NPs. This result demonstrated that this method may design a new and green strategy for synthesizing the well-defined morphologies, compositions, and sizes of the hybrid nanomaterial for photocatalytic hydrogen generation, photocatalytic CO_2 reduction and photosynthesis of organic molecules.

1. Introduction

Photoelectrochemical (PEC) water splitting has been regarded as one of the most promising strategy to convert solar energy to hydrogen [1–5]. TiO_2 was applied as the photoanode since it was firstly discovered in 1972 by Fujishima and Honda [6]. Nowadays, TiO_2 has attracted soaring interest as an efficient photoanode due to its abundance, low cost and chemical stability [7–10]. Among numerous types of TiO_2 nanostructures, the one-dimensional (1D) TiO_2 semiconductor nanostructures such as nanowires and nanorods have aroused extensive attention owing to their advantages in high specific surface areas and efficient optical absorption. 1D nanostructures can shorten the migration distance of photogenerated holes from bulk to the surface of materials and provide direct electron transmission channels for electrons migration [11–13]. However, the high recombination rates of the photogenerated electrons and holes hinder the utilization of quantum efficiency in photocatalysis [14]. Various strategies have been concentrating on the TiO_2-based semiconductor to enhance the efficiency of photocatalytic conversion, such as element doping [15,16], structural modifications [17] or constructing heterostructures [18,19]. Recently, it is reported that the modification of TiO_2 by coupling with noble metal nanoparticles is a promising method to improve the photocatalytic of TiO_2 [20,21]. The noble metal Pd is considered to be one of the most effective candidates for hydrogen evolution and coupling reactions. The metal particles contact with the semiconductor metal oxide can cause energy state difference of work function. When Pd nanoparticles are coupled with semiconductor, the electrons will flow to the precious metals with lower Fermi energy level until they have the same Fermi energy level. In the case of illumination, the excited electrons transfer to the surface of the noble metal to form the Schottky barriers between the TiO_2 and the noble metal, which prevents the recombination of the photo-generated electron-hole pairs and promotes efficient charge separation [22]. The semiconductor with smaller size of the metal particles will reduce metal-semiconductor barrier height and have a higher Schottky barrier. Therefore, in the noble metal–semiconductor heterostructures system, controllable

* Corresponding author.
E-mail address: gaolu@jlu.edu.cn (L. Gao).

https://doi.org/10.1016/j.jallcom.2019.01.196
0925-8388/

assembly of composites is the key to obtain high catalytic activities and understand the interaction between them. Large of methods have been prepared to synthetize tuneable particles with narrow size distribution and well-dispersion supported on TiO_2, such as electrochemical deposition [23], deposition–precipitation [24,25], dip coating [26] and photoreduction (PR) method [27]. Some methods are simple but represent the low control of the dispersion and particle size. To avoid the aggregation of nanoparticles, surfactants or stabilizers are usually used as capping agents to stabilize nanoparticle, thus limiting their chemical activity. Furthermore, most composite material generally needs to control complex synthesis conditions and expensive equipment to produce noble metal particles with small size on semiconductor surface [28].

Herein, we design an innovative electrode with one-dimensional TiO_2 nanowires modified with Pd nanoparticles (NPs) for PEC water splitting by Electrospray (ES) technique. ES has been used widely to fabricate charged and dispersive microdroplets in a high voltage electric field [29–31]. Without using any reducing agents and surfactants, the controllable Pd nanoparticles of the size, structures can be obtained by changing the deposition conditions. In this work, small-sized Pd NPs decorated with TiO_2 NWs was successfully fabricated by ES technique for the first time and the sample showed high PEC performance. Moreover, our present work will offer a new strategy for the preparation of semiconductor noble metal composite nanostructure and the application for solar energy to hydrogen.

2. Experimental

2.1. Preparation of TiO_2 nanowires

Rutile TiO_2 nanowire arrays (NWs) were grown on Fluorine-doped tin oxide (FTO) glass substrate by the hydrothermal method [32]**.** First, the FTO glass were ultrasonically pre-cleaned in sequence of acetone, ethanol and de-ionized water each for 20min. Then, they were dried in N_2 gas flow. FTO glasses were immersed in 25 mM $TiCl_4$ aqueous solution and then put in the oven at 70 °C for 30 min to form TiO_2 seed. The seed was annealed in air at 450 °C for 1 h. 5 mL of concentrated hydrochloric acid was diluted with 5 mL deionized (DI) water and stirred for 15 min. 0.15 mL titanium *n*-butoxide was added in the mixture to form precursor solution. The clean FTO glass substrate was submerged in the solution with an angle against the wall of the Teflon-lined stainless steel autoclave (18 mL volume). Then, the precursor solution was transferred to autoclave. The sealed autoclave was heated in an electric oven at 150 °C for 6 hours. The sample was thoroughly washed with ethanol, distilled water and dried in air slowly. A white TiO_2 nanowire film was uniformly coated on the FTO glass substrate. Finally, the sample was annealed in air at 550 °C for 2 h to improve the crystallinity of the rutile TiO_2.

2.2. Synthesis of the of Pd nanoparticles decorated TiO_2 nanowire arrays

Pd nanoparticles decorated TiO_2 nanowire arrays were deposited using a self-made equipment (Fig. S1), including an injection pump (Kent Scientific Corporation, USA), pressure control module (Boher High Voltage Power Supplies Co., Ltd, China) and a plate heater with a three dimensional operating platform. The FTO conductive glass with TiO_2 nanowire array was used as the receiving board to form a closed circuit. The crystal growth temperature can be controlled by the heating controller. 0.001 M palladium acetate ($Pd(Ac)_2$) was dissolved in acetonitrile under vigorous stirring for 30 min to make solution homogeneous. The amount of Pd NPs was achieved by controlling the volume of the precursor solution. In this experiment, the solution flow rate was set as 5 μL min^{-1} and precursor solution was 100–400 μL. The atomizer flow rate was 0.5 MPa. The capillary voltage is set as 10 kV to produce charged micro-droplets. The distance from the substrate to the needle tip is 50 mm. Finally, the Pd nanoparticles were deposited on the TiO_2 nanowire arrays via the electrospray method.

2.3. Characterization

The crystalline phase was characterized by X-ray diffractometer (XRD) with Cu Ka radiation. Surface morphology, structure and chemical composition were measured with Helios Nanolab 600i scanning electron microscopes (SEM), energy dispersive spectroscopy (EDS), and transmission electron microscopy (TEM and X-ray photoelectron spectroscopy (XPS). The UV–Vis spectra measurements were carried out using a Shimadzu U-4100 spectrophotometer.

2.3.1. Photoelectrochemical measurements

PEC performances were measured by a three-electrode system (CH Instruments, CHI 660D). Pristine TiO_2 and Pd NPs modified TiO_2 nanowire arrays were served as the working electrode, Ag/AgCl electrode as the reference electrode and the platinum wire as the counter electrode. 1 M NaOH aqueous solution (pH = 13.6) was used as the electrolyte. A 450-W Xenon lamp was designed as the light source during the PEC performance measurements. The light intensity was calibrated to 100 mW cm^{-2}. To convert the measured potentials Ag/AgCl to the reversible hydrogen electrode (RHE) scale, Nernst equation was used as follows:

$$E_{RHE} = E_{Ag/AgCl} + 0.059\ pH + E^0 Ag/AgCl$$

where $E_{Ag/AgCl}$ stands for the measured potential against the reference electrode and $E^0_{Ag/AgCl} = 0.1976$ V at 25 °C. The illuminated area of the working electrode was 0.502 cm^2. The linear-sweep voltammogram was measured with a scan rate of 10 mV s^{-1} and transient photocurrent density versus time plots was applied at the potential of 0.23 V vs. Ag/AgCl with an illumination on/off interval of 210 s. IPCE spectra was measured with a simulated sunlight and cut filters ranging from 350 nm to 550 nm. Electrochemical impedance spectroscopy (EIS) measurements were tested to scrutinize the interfacial properties between the electrode and the electrolyte through an Electrochemical Workstation (ZAHNER, Germany), the electrolyte over the frequency ranging from 0.1 Hz to 100 kHz with an AC voltage of 0.3 V under the light illumination. The Mott–Schottky plots were achieved at a frequency of 1000 Hz in the dark.

3. Results and discussion

The procedure developed for fabricating rutile TiO_2 nanowires on FTO substrate and then decorated with Pd NPs to form hybrid structure is illustrated in Fig. 1(a–c). Briefly, TiO_2 NWs were grown on the FTO using the hydrothermal method, then Pd nanoparticles were deposited on the TiO_2 via the electrospray method. The cross section of TiO_2 nanowire array indicated that the length of TiO_2 nanowire is about 2 μm. Fig. 1(e) and (f) show the SEM images of the pristine TiO_2 and Pd/TiO_2 hybrid nanomaterial. Pd NPs with an average size of about 5 nm were uniformly loaded on the surface of TiO_2 nanowires.

Fig. 2(a) shows the XRD patterns of the TiO_2 NWs before and after deposition of the Pd nanoparticles. For TiO_2 NWs, except for the phase of SnO_2 of FTO substrate (JCPDS 41-1445), the sample shows the characteristic diffraction peaks of tetragonal rutile phase

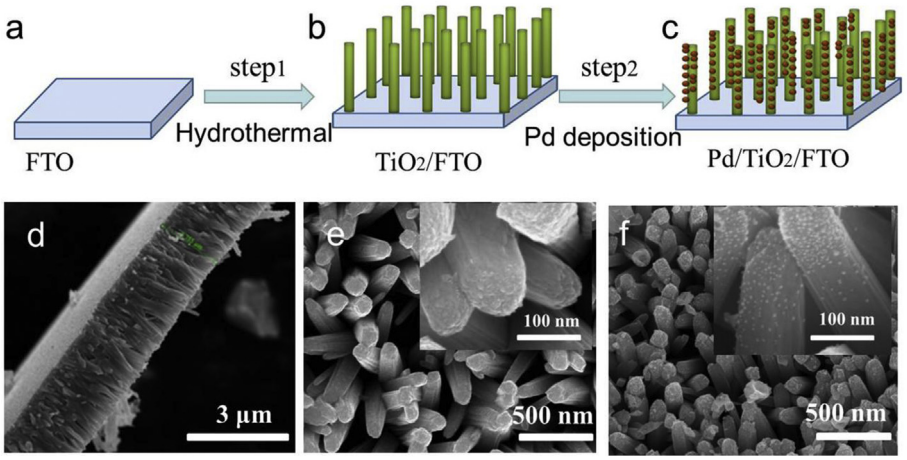

Fig. 1. (a–c) Schematic diagram of the Pd/TiO_2 fabrication procedure (d) The cross section of TiO_2 nanowire SEM images of the (e) pristine TiO_2 NWs (f) Pd NPs modified with TiO_2 NWs.

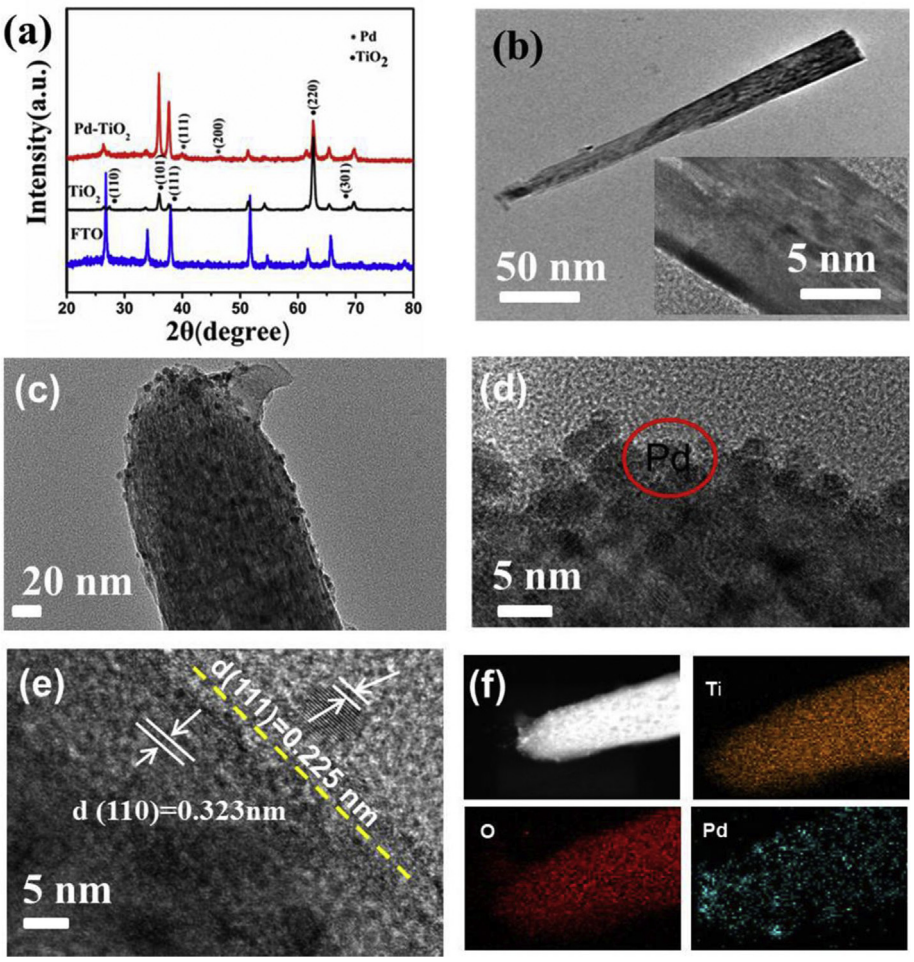

Fig. 2. (a) XRD patterns of TiO_2 and Pd-TiO_2 (b) TEM images of the TiO_2 NWs.(c) Low-magnification and (d) (e)high-resolution TEM images of Pd-TiO_2 hybrid nanostructure (f) EDS element mapping images of a single Pd-TiO_2, showing the distributions of Ti, O, and Pd.

(JCPDS 21-1276). The peak intensity of (002) was higher than other diffraction peaks, indicating that the TiO_2 nanowires grow along the crystal plane and have the preferred orientation of [001]. The two peaks were observed at 40.0°, 46.5° in the Pd/TiO_2 corresponding to the (111), (200) planes, which indicates the metallic Pd particles (JCPDS 88-2335) dispersed on the surface of TiO_2 NWs. To further investigate the size of Pd nanoparticles and the hybrid nanostructure, TEM is also carried out. Fig. 2(b) shows a

typical low magnification transmission electron microscopy (TEM) image of the single TiO_2 nanowire. The TiO_2 nanowires have triangular ends, smooth surfaces and uniform thickness. The mean diameter and length of the TiO_2 nanowires is about 100 nm and 2 μm. As can be seen from Fig. 2(c), the Pd nanoparticles with an average size distribution of about 5 nm were homogenously dispersed on the TiO_2 nanowires. The average lattice spacing of 0.323 nm was correspond to the (110) crystalline plane of rutile TiO_2, while the lattice spacing of 0.225 nm can be rooted in the (111) plane of the Pd nanocrystal, together confirming the decoration of Pd nanoparticles on the surfaces of the TiO_2 nanowires. In addition, TEM and HRTEM images clearly show that Pd NPs grow closely on the surface of TiO_2 nanowires and exhibit a clear interface between them. The EDS element-mapping further confirmed the structural feature of Pd nanoparticles distribution on the TiO_2 surface.

The elemental composition and chemical environment of Pd/TiO_2 hybrid structure nanocomposites were analysed by X-ray photoelectron spectroscopy (XPS). The full survey spectrum of the Pd/TiO_2 indicated the presence of Pd, Ti and O elements. In the Ti 2p region, the binding energies of Ti $2p_{1/2}$ and Ti $2p_{3/2}$ were located at 464.3 eV and 458.6 eV, which matched well with the typical values of TiO_2. Notably, as shown in Fig. 3(b), the Ti 2p peak exhibit a positive shift of 0.3 eV from pristine TiO_2 to Pd/TiO_2, which demonstrated the electron transfer between Pd and TiO_2 [33]. The Pd 3d XPS spectrum was fitted to two peaks at 334.8 eV (Pd $3d_{5/2}$) and 340.1 eV (Pd $3d_{3/2}$) with a distance of approximately 5.3 eV, revealing that Pd^0 mainly exists on the TiO_2 nanowire surface [34]. Fig. 4(d) displays the O 1s XPS spectra, the binding energy at 529.6 eV could be assigned to typical of metal-oxygen bonds, the O 1s sitting at 531.2 eV could be assigned to the Ti—OH [33].

To investigate Pd nanoparticles decorated TiO_2 nanowires on the catalyst activity, the photocurrent density was obtained. Fig. 4(a) shows that the photocurrent density has been greatly increased than pristine TiO_2. The current density of pure TiO_2 and Pd-TiO_2 photoanodes is close zero in the dark current, indicating all sample electrodes cannot be excited the separation of electrons and holes even at the high potential. The photocurrent density of Pd/TiO_2 photoanode is significantly enhanced and the onset potential is declined than that of the pure TiO_2. It is proved that Pd NPs play an effective role in photoactivity and facilitate the separation of photogenerated electrons and holes under illumination. The photocurrent intensity of the Pd/TiO_2 is 1.4 mA cm^{-2} (at 1.23 V vs. RHE), which was more than five times higher than the pristine TiO_2 (0.25 mA cm^{-2}). Fig. S3 shows the UV—Vis spectra for the TiO_2 and Pd/TiO_2 photoanode over a wavelength range from 300 to 800 nm. The diffuse reflectance spectrum of the pristine TiO_2 showed a prominent absorption edge at 400 nm equivalent to an energy bandgap of 3.0 eV, which are in consistent with previous reports of the rutile TiO_2 [35]. When TiO_2 NWs decorated with Pd NPs, the resulting photoanode did not show obvious change in light absorption. It only exhibited a slight red shift about the UV—Visible absorption and wider band edge absorption. We thus conclude that the enhanced PEC performance of Pd/TiO_2 photoanode does not caused by the light absorbance. In addition, the photocurrent stability of the electrodes is also an important factor for efficient PEC hydrogen production system. Fig. 4(c) shows the photocurrent of the Pd/TiO_2 electrode at the potential of 1.23 V vs RHE under illumination. The Pd/TiO_2 photoanode exhibits a very stable photo response with 2000s, implying the high stability of the electrode.

Incident-photon-to-current-conversion efficiency (IPCE) tests (Fig. 4(d)) were also performed to confirm the mechanism of enhanced PEC of the TiO_2 NWs and Pd/TiO_2 photoanodes. The IPCE

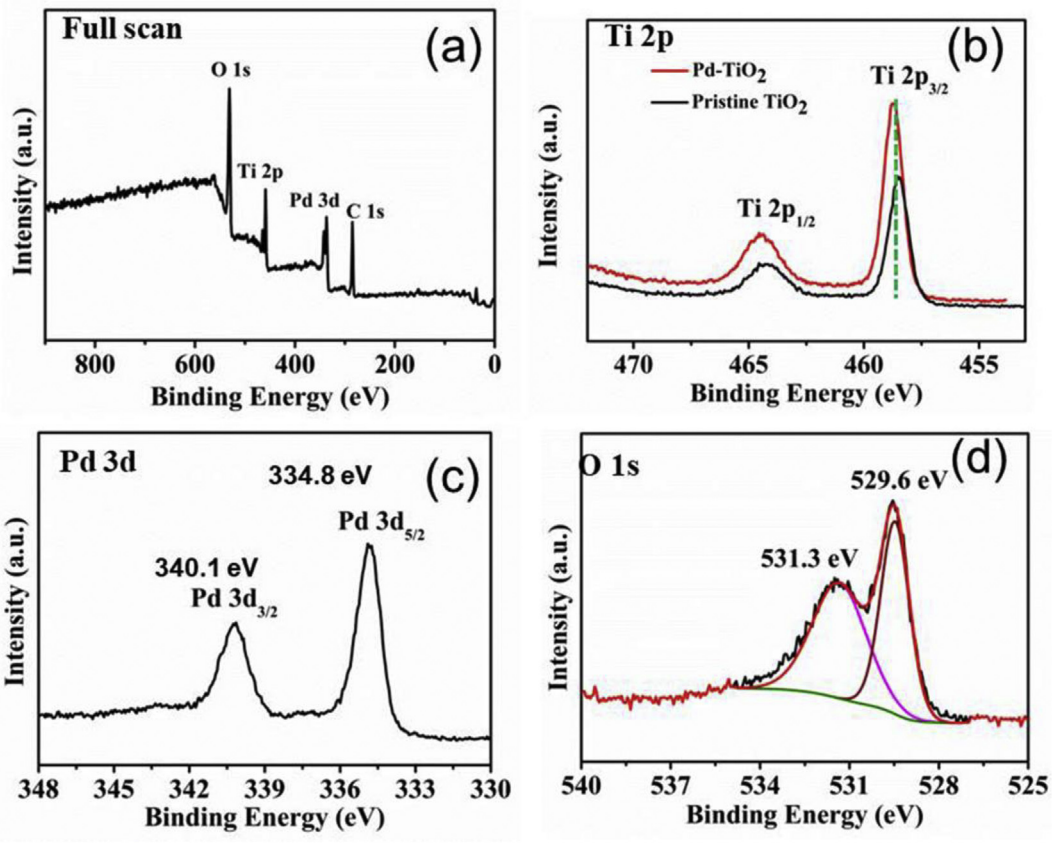

Fig. 3. (a) XPS spectra of the Pd/TiO_2hybrid structure: (a) Full spectrum, (b) Ti 2p, (c) Pd 3d and (d) O 1s.

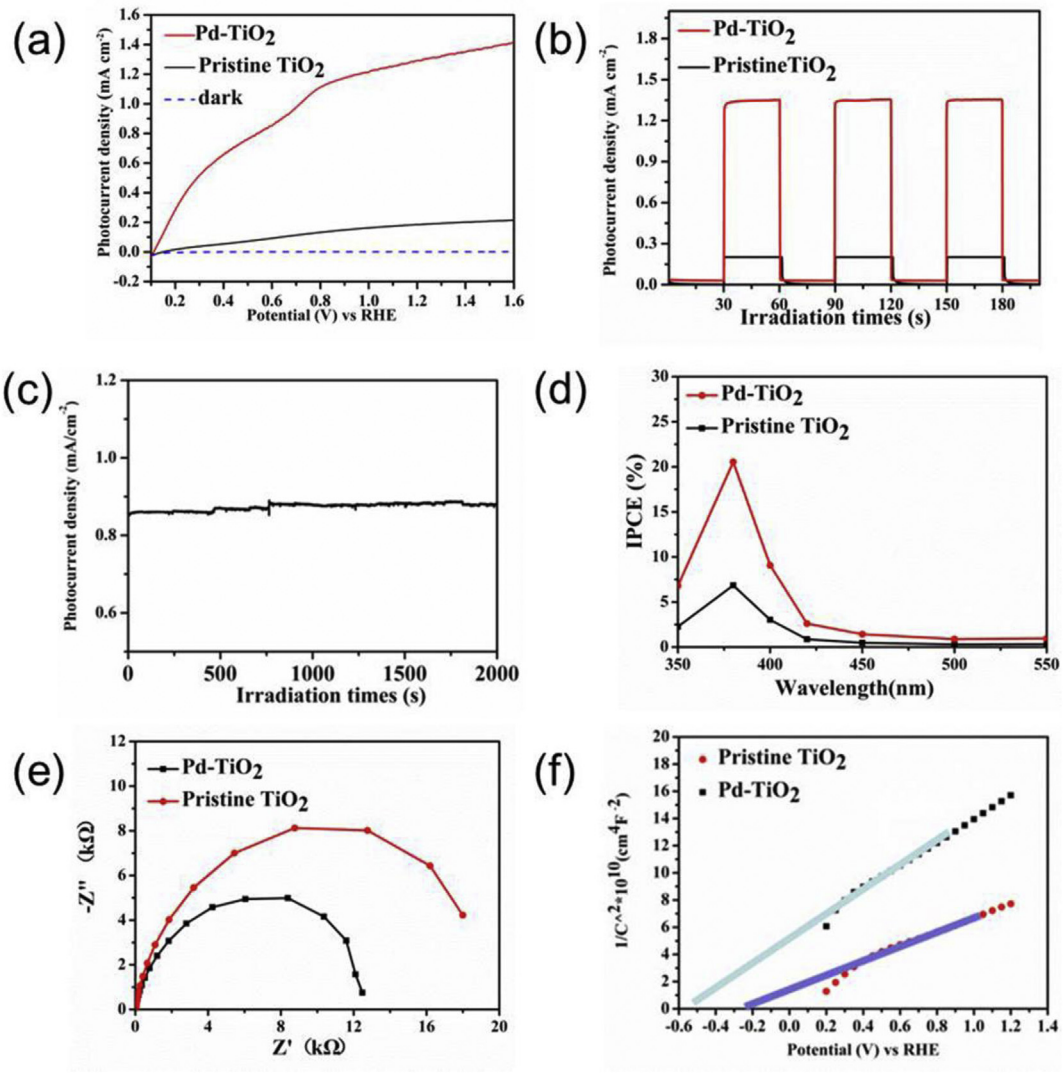

Fig. 4. (a) Linear-sweep voltammograms of pristine TiO_2 and Pd-TiO_2 photoanodes (b) Chronoamperometry measurements of the photoanodes at an external potential of 1.23 V vs. RHE (c) Photocurrent of the Pd/TiO_2 electrode at the potential of 1.23 V vs RHE under AM1.5 illumination for 2000 s (d) IPCE spectra measured at 1.23 vs. RHE (e) electrochemical impedance spectra (f) Mott–Schottky plots of pristine TiO_2 and Pd-TiO_2 photoanodes.

spectrum of each electrode was scanned from 350 to 550 nm at a potential of 1.23 V. IPCE was calculated applying the following expression:

$$\mathrm{IPCE} = 1240\,\mathrm{J}\Big/(\lambda \mathrm{P_{light}})$$

where J refers to photocurrent density (mA cm^{-2}), P_{light} is the irradiance intensity of the illumination power (mW cm^{-2}) and λ is the incident light wavelength (nm). As reveled in Fig. 4(d), the IPCE at 380 nm increases from 6% to 22% after the Pd nanoparticles coated TiO_2 NWs. The enhancement can be interpreted as the Pd NPs promoted the charge transport at the electrode/electrolyte interface for water splitting. In Fig. 4(e), the electrochemical impedance measurements (EIS) under light illumination were carried out to estimate the overall charge transfer of TiO_2 NWs and Pd/TiO_2. In Nyquist diagrams, the smaller curve radius is usually corresponding to the small charge transfer resistance between the electrode and electrolyte interface. It can be clearly seen that the Pd/TiO_2 photoanode in the arc diameters in the Nyquist plot is smaller than the TiO_2 NWs, indicating the high carrier transmission efficiency in the composite photoelectrode. The Mott–Schottky plot can give us more information about charge carrier transportation properties of semiconductor electrode. A positive slope was shown in the samples from the Mott-Schottky plots, which shows the n-type semiconductor. The smaller Mott–Schottky slope of the Pd/TiO_2 photoanode also shows the faster rate of charge transfer. The flat-band potential can be calculated by the following equation:

$$1\Big/C^2 = (2\Big/_{e\varepsilon\varepsilon_0}\mathrm{Nd})[E - E_{FB} - kt/e)$$

wherein e is the electron charge (1.6×10^{-19}), ε is the relative permittivity of rutile TiO_2 ($\varepsilon = 170$), ε_0 is the permittivity of vacuum (ε_0=8.86×10^{-14} F cm^{-1}), Nd is the carrier density, E is the electrode potential, E_{FB} is the flatband potential, k is Boltzmann's constant and T is the temperature [35]. In addition, the calculated carrier densities of the pristine TiO_2 and Pd/TiO_2 photoanode were 9.43×10^{18} cm^{3-} and 1.43×10^{19} cm^{3-} respectively. The higher donor density improves the charge transport and carrier transfer, which provides strong evidence for the enhanced PEC performance.

Fig. 5(a) shows a set of the I-V curves of the pristine TiO_2nanowire array electrodes and TiO_2 NWs that were decorated with different precursor contents of Pd NPs. The density of Pd NPs can be controlled by adjusting the amount of the precursor solution. With increasing the deposition volume, the amount of Pd nanoparticles was increased rapidly. Fig. S2 shows the SEM images of the TiO_2 nanowires depositing with different concentration of the Pd NPs. In order to determine the existence of Pd nanoparticles and the Pd-TiO_2 ratio in Pd/TiO_2 hybrid structure, X-ray spectroscopy (EDS) was also employed. Significantly, the photocurrent density of TiO_2 nanowires that were loaded with Pd NPs (200 μL) showed the optimum performance. When the deposition amounts further increases, the photocurrent density gradually decreases. This phenomenon can be attributed to large amounts of Pd NPs may prevent the light from entering the TiO_2 surface and reduce the photocurrent generation. The high coverage of Pd NPs will also decrease the specific surface area of TiO_2 in direct contact with the electrolyte, thus affecting the oxidation performance of water. Fig. 5(b) reveals the plot of the obtained photocurrent density as a function of the Pd-TiO_2 photoanode with various Pd/Ti atomic ratio. It is concluded that for getting the best PEC performance, the atomic ratio was 0.015. The photocurrent density of the Pd/TiO_2 photoanodes prepared at different substrate temperatures was also indicated in Fig. 5(c). Photocurrent density was observed to rise with increasing the substrate temperatures. The Pd/TiO_2 photoanodes at 450 °C showed optimum performance. At 1.23 V vs. RHE, the photocurrent of the Pd/TiO_2 prepared at 450 °C is 1.4 mA cm^{-2}, which is 2.5 times than the Pd/TiO_2 prepared at 350 °C. Additionally, the enhanced photoactivity could be attributed to narrower size distribution (Fig. 6), which provides a large surface area to contact with the electrolyte/electron diffusion and facilitate the charge transport and collection, therefore reducing the photogenerated carriers and holes recombination. Moreover, the small size of the metal nanoparticles will promote the raise of work function due to the quantum size effect. The Schottky barrier height will make it more difficult to transfer carriers from semiconductor to metal. Thus prolong the lifetime of the carrier to enhanced catalytic activity. The mean diameter of Pt NP varied from 8 nm to 3 nm when the substrate changed from 350 °C to 450 °C. With the increasing of the substrate temperature, the evaporation rate of the solvent is accelerated, resulting in smaller microdroplets and smaller nanoparticles. As reveled in Fig. 5(c), the electrochemical impedance spectroscopy (EIS) analysis of Pd/TiO_2 photoanodes was further carried out to prove the interfacial charge transfer resistance. The semi-circular diameter is usually corresponded with the photoactivities well in the Nyquist plot. Obviously, the diameters of the semicircle of Pd/TiO_2 photoanodes prepared at 450 °C is smaller than the those of obtained at other temperatures, suggesting the fastest charge transfer kinetics at the electrode/electrolyte interface.

4. Conclusion

In summary, a novel Pd/TiO_2 hybrid nanomaterial was successfully synthesized by a facile low-cost method. The Pd/TiO_2 obtained a high photocurrent density of 1.4 mA cm^{-2} at the potential of 1.23 V vs. RHE, which was more than five times higher than the pristine TiO_2. The IPCE is 22% for Pd/TiO_2 photoanode and 6% for pristine TiO_2 photoanode at 380 nm. Decorating Pd nanoparticles with narrow size distribution on the TiO_2 nanowires form Schottky junction, thus promotes the separation of the photogenerated electrons to boost the hydrogen generation efficiency. By simply varying the deposition amount and substrate temperature, the size and number of deposited Pd nanoparticles can be

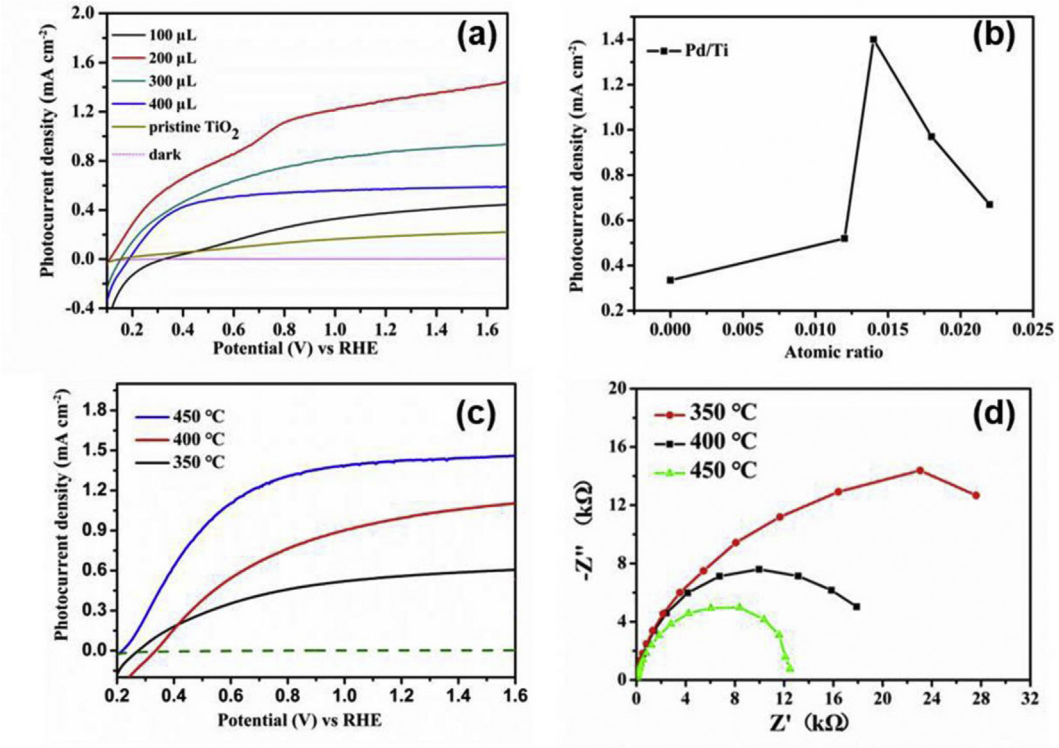

Fig. 5. (a) Linear-sweep voltammograms of Pd-TiO_2 photoanodes with different content of Pd nanoparticles (b) Plot of the obtained photocurrent density as a function of the Pd-TiO_2 photoanodes photoanode with various Pd/Ti atomic ratio(c) Photocurrent–potential curves and (d) electrochemical impedance spectra of Pd/TiO_2 photoanodes with different substrate temperatures.

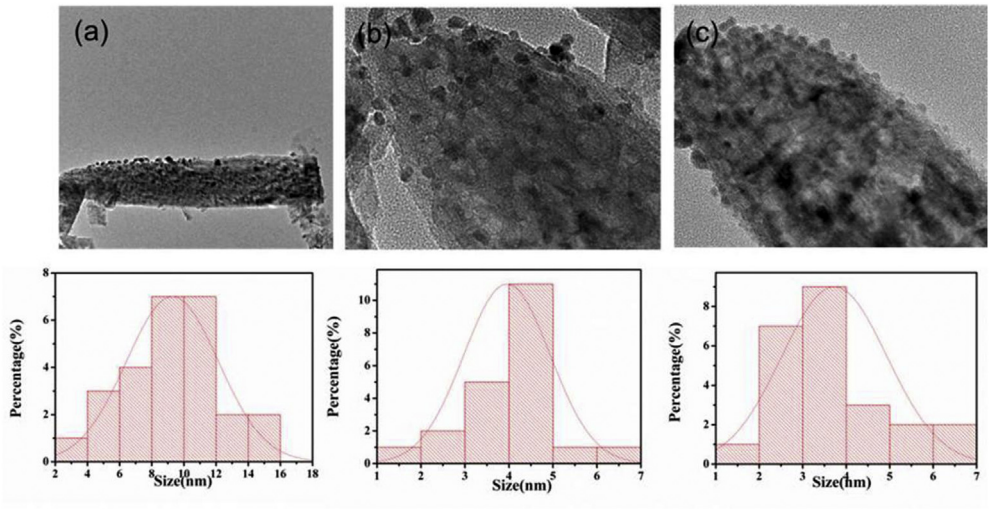

Fig. 6. TEM images and the size distribution of the Pd/TiO_2 prepared at different substrate temperatures (a) 350 °C (b) 400 °C (c) 450 °C.

controlled accurately. The substrate temperature has a significant effect on the size distribution and PEC properties. The content of the Pd nanoparticles on the TiO_2 nanowires surface determines the charge transfer at the photoanode/electrolyte interface and quality of the PEC performance. The results show that photoanodes deposited at 450 °C, the content of the precursor solution of 200 μL revealed the best PEC water splitting photocurrent. It was possible to increase the PEC activity by manipulating the nanostructure by changing the size structure and composition. More importantly, we provided a promising strategy to fabricate metal-semiconductor systems photoelectrodes to synergistically enhance the catalytic activity.

Acknowledgements

This work was supported by National Nature Science Foundation of China (grants 21427802, 21671076 and 21621001).

Appendix A. Supplementary data

Supplementary data to this article can be found online at https://doi.org/10.1016/j.jallcom.2019.01.196.

References

[1] W. Wang, J. Dong, X. Ye, Y. Li, Y. Ma, L. Qi, Small 12 (2016) 1469–1478.
[2] F.-X. Xiao, J. Miao, H.-Y. Wang, H. Yang, J. Chen, B. Liu, Nanoscale 6 (2014) 6727–6737.
[3] Y. Zhao, M. Han, H.X. Wang, C.C. Chen, J. Chen, Inorg. Chem. Front. 3 (2016) 1536–1542.
[4] C. Chen, J. Cao, Q.Q. Lu, X.Y. Wang, L. Song, Z.Q. Niu, J. Chen, Adv. Funct. Mater. 27 (2017), 1604639.
[5] J. Hou, H. Cheng, O. Takeda, H. Zhu, Energy Environ. Sci. 8 (2015) 1348–1357.
[6] Fujishima, K. Honda, Nature 238 (1972) 37–38.
[7] N. Liu, C. Schneider, D. Freitag, E.M. Zolnhofer, K. Meyer, P. Schmuki, Chem. Eur. J. 22 (2016) 13810–13814.
[8] Z. Sun, M. Liang, J. Chen, Accounts Chem. Res. 48 (2015) 1541–1550.
[9] C. Mao, F. Zuo, Y. Hou, X. Bu, P. Feng, Angew. Chem. Int. Ed. 53 (2014) 10485–10489.
[10] Y. Hou, X.-Y. Li, Q.-D. Zhao, X. Quan, G.-H. Chen, Adv. Funct. Mater. 20 (2010) 2165–2174.
[11] X. Feng, K. Shankar, O.K. Varghese, M. Paulose, T.J. Latempa, C.A. Grimes, Nano Lett. 8 (2008) 3781–3786.
[12] R. Abe, J. Photochem. Photobiol. C 11 (2010) 179–209.
[13] Z. Wang, M. Cao, L. Yang, D. Liu, D. Wei, Analyst 142 (2017) 2805–2811.
[14] H.-i. Kim, D. Monllor-Satoca, W. Kim, W. Choi, Energy Environ. Sci. 8 (2015) 247–257.
[15] L. Kong, Z. Jiang, T. Xiao, L. Lu, M.O. Jones, P.P. Edwards, Chem. Commun. 47 (2011) 5512–5514.
[16] D.H. Kim, K.S. Lee, Y.S. Kim, Y.C. Chung, S.J. Kim, J. Am. Ceram. Soc. 89 (2006) 515–518.
[17] S. Cho, Z. Chen, A.J. Forman, D.R. Kim, P.M. Rao, T.F. Jaramillo, X. Zheng, Nano Lett. 11 (2011) 4978–4984.
[18] N. Wu, J. Wang, D.N. Tafen, H. Wang, J.G. Zheng, J.P. Lews, X. Liu, S.S. Leonard, A. Manivannan, J. Am. Chem. Soc. 13 (2010) 26679–26685.
[19] Pan, Y. Dong, W. Zhou, Q. Pan, Y. Xie, T. Xie, G. Tian, G. Wang, ACS Appl. Mater. Interfaces 5 (2013) 8314–8320.
[20] E. Kowalska, O.O.P. Mahaney, R. Abe, B. Ohtani, Phys. Chem. Chem. Phys. 12 (2010) 2344–2355.
[21] E. Grabowska, M. Marchelek, T. Klimczuk, G. Trykowski, A. Zaleska-Medynska, J. Mol. Catal. A Chem. 423 (2016) 191–206.
[22] W.J. An, W.N. Wang, B. Ramalingam, S. Mukherjee, B. Daubayev, S. Gangopadhyay, P. Biswas, Langmuir 28 (2012) 7528–7534.
[23] T.C. Damato, C.C.S. de Oliveira, R.A. Ando, P.H.C. Camargo, Langmuir 29 (2013) 1642–1649.
[24] W.F. Yan, S.M. Mahurin, Z.W. Pan, S.H. Overbury, S. Dai, J. Am. Chem. Soc. 127 (2005) 10480–10481.
[25] S. Pany, B. Naik, S. Martha, K. Parida, ACS Appl. Mater. Interfaces 6 (2014) 839–846.
[26] D.B. Ingram, S. Linic, J. Am. Chem. Soc. 133 (2011) 5202–5205.
[27] S.F. Chen, J.P. Li, K. Qian, W.P. Xu, Y. Lu, W.X. Huang, S.H. Yu, Nano Res. 3 (2010) 244–255.
[28] X. Chen, G. Wu, J. Chen, X. Chen, Z. Xie, X. Wang, J. Am. Chem. Soc. 133 (2011) 3693–3695.
[29] H. Fang, K. Huang, L. Yuan, X. Wu, D. Wang, H. Chen, S. Feng, New J. Chem. 40 (2016) 7294–7298.
[30] J. He, Y. Sun, M. Wang, Z.B. Geng, X.F. Wu, L. Wang, H.W. Chen, K.K. Huang, S.H. Feng, J. Alloys Compd. 752 (2018) 389–394.
[31] Wang, X. Wu, K. Huang, Y. Sun, Y. Zhang, H. Zhang, J. He, H. Chen, J. Ding, S. Feng, Nanoscale 10 (2018) 6678–6683.
[32] X. Zhang, Y. Liu, S.-T. Lee, S. Yang, Z. Kang, Energy Environ. Sci. 7 (2014) 1409–1419.
[33] F. Su, T. Wang, R. Lv, J. Zhang, P. Zhang, J. Lu, J. Gong, Nanoscale 5 (2013) 9001–9009.
[34] Q. Fu, T. Wagner, S. Olliges, J. Phys. Chem. B 109 (2005) 944–951.
[35] Wang, Y. Wang, P. Schmuki, S. Kment, R. Zboril, Electrochim. Acta 260 (2018) 212–220.